Integrated strategy for improving functional connectivity mapping using multiecho fMRI

Prantik Kundu[a,b,1], Noah D. Brenowitz[a], Valerie Voon[b], Yulia Worbe[b], Petra E. Vértes[b], Souheil J. Inati[c], Ziad S. Saad[d], Peter A. Bandettini[a,c,2], and Edward T. Bullmore[b,e,f,2]

[a]Section on Functional Imaging Methods, [c]Functional MRI Core Facility, and [d]Statistical and Scientific Computing Core, National Institute of Mental Health, Bethesda, MD 20814; [b]Behavioural and Clinical Neuroscience Institute, University of Cambridge, Cambridge CB2 1QP, United Kingdom; [e]National Institute of Health Research Cambridge Biomedical Research Centre, Cambridgeshire Peterborough National Health System Foundation Trust, Cambridge SW1A 2NS, United Kingdom; and [f]Clinical Unit Cambridge, GlaxoSmithKline, Cambridge CB2 0QQ, United Kingdom

Edited by Marcus E. Raichle, Washington University in St. Louis, St. Louis, MO, and approved July 31, 2013 (received for review January 29, 2013)

Functional connectivity analysis of resting state blood oxygen level–dependent (BOLD) functional MRI is widely used for noninvasively studying brain functional networks. Recent findings have indicated, however, that even small (≤1 mm) amounts of head movement during scanning can disproportionately bias connectivity estimates, despite various preprocessing efforts. Further complications for interregional connectivity estimation from time domain signals include the unaccounted reduction in BOLD degrees of freedom related to sensitivity losses from high subject motion. To address these issues, we describe an integrated strategy for data acquisition, denoising, and connectivity estimation. This strategy builds on our previously published technique combining data acquisition with multiecho (ME) echo planar imaging and analysis with spatial independent component analysis (ICA), called ME-ICA, which distinguishes BOLD (neuronal) and non-BOLD (artifactual) components based on linear echo-time dependence of signals—a characteristic property of BOLD T_2^* signal changes. Here we show for 32 control subjects that this method provides a physically principled and nearly operator-independent way of removing complex artifacts such as motion from resting state data. We then describe a robust estimator of functional connectivity based on interregional correlation of BOLD-independent component coefficients. This estimator, called independent components regression, considerably simplifies statistical inference for functional connectivity because degrees of freedom equals the number of independent coefficients. Compared with traditional connectivity estimation methods, the proposed strategy results in fourfold improvements in signal-to-noise ratio, functional connectivity analysis with improved specificity, and valid statistical inference with nominal control of type 1 error in contrasts of connectivity between groups with different levels of subject motion.

resting state fMRI | human neuroimaging | time series

Resting state experiments typically involve a short period (i.e., 10 min) of blood oxygen level–dependent (BOLD) functional MRI (fMRI) scanning while participants lie in the scanner without experimental control over brain function. The data show low-frequency ($f \leq 0.1$ Hz) oscillations indicative of spontaneous brain activity. Functional connectivity between brain regions is then typically estimated by the correlation between time series (1). Unfortunately, resting state fMRI is highly susceptible to artifacts. It has recently been shown that small (≤1 mm) and transient movements of the subject's head during scanning can bias estimates of time series correlation for long distance anatomical connections, even after the data have been preprocessed by traditional methods (2–4). The effects of head motion and related artifacts are problematic especially for studies of very young or elderly subjects or patients with neuropsychiatric disorders, all of whom demonstrate a greater extent of head movement than healthy adults.

Current proposals for solving problems related to motion artifact involve elaborating traditional methods for "denoising" the BOLD fMRI signal time series acquired at one optimized echo time (TE) (5). One denoising step that has been widely adopted is to regress the raw fMRI time series to the series of head motion parameters estimated post hoc as translations and rotations in three spatial dimensions to geometrically align all fMRI volumes to a reference volume. Additional "nuisance" regressors are often included in regression models, such as the global mean fMRI time series and/or time series representing presumably nonneuronal signal of the white matter or CSF (6, 7). Before or after regression analysis, time series are typically also band-pass filtered to remove higher-frequency signals considered less likely to represent functionally related variance (8). Some groups prefer to use independent component analysis (ICA) to decompose the time series into spatially independent components and remove components identified as artifacts by user-dependent evaluation of anatomical localization and/or time series. Finally, it has been suggested that in extreme cases, time points that are severely contaminated by otherwise intractable movement effects may be simply deleted or "scrubbed" from the time series (2). Although some permutation of these preprocessing steps can indeed substantially reduce contamination of the data by nonneuronal sources, this is not achieved without cost. All of these denoising operations will have a major impact on the statistical properties of the data by varying the degrees of freedom in a poorly controlled way or introducing time series artifacts due to preprocessing. Altogether, traditional preprocessing often implements several arbitrary operator-dependent choices and therefore may be incompletely effective.

Here, we advocate a more radical departure from conventional resting state fMRI methodology using an integrated procedure for data acquisition, BOLD denoising, and connectivity estimation and statistical inference. Using our previously published method combining multiecho (ME) echo planar imaging (EPI) and ICA, called ME-ICA, fMRI signals are acquired at multiple TEs, and BOLD signals are identified as independent components having linearly TE-dependent percent signal changes, which is a distinctive characteristic of BOLD T_2^* (transverse susceptibility-weighted relaxation rate) signal (9–11). Component-level TE dependence of BOLD signals is measured using the pseudo-F-statistic κ; components that scale strongly with echo time, indicating BOLD weighting, will have high κ scores. In contrast, component-level TE independence can be

Author contributions: P.K., V.V., Y.W., P.E.V., S.J.I., Z.S.S., P.A.B., and E.T.B. designed research; P.K., V.V., and Y.W. performed research; P.K., N.D.B., Z.S.S., and E.T.B. contributed new reagents/analytic tools; P.K. and P.E.V. analyzed data; and P.K., P.E.V., Z.S.S., P.A.B., and E.T.B. wrote the paper.

The authors declare no conflict of interest.

This article is a PNAS Direct Submission.

Data deposition: The data reported in this paper have been posted in the Neuroimaging Informatics Tools and Resources Clearinghouse (http://www.nitrc.org/) with the project name ME-ICR.

[1]To whom correspondence should be addressed. E-mail: kundup@mail.nih.gov.

[2]P.A.B. and E.T.B. contributed equally to this work.

This article contains supporting information online at www.pnas.org/lookup/suppl/doi:10.1073/pnas.1301725110/-/DCSupplemental.

Downloaded from https://www.pnas.org by 117.98.129.62 on December 26, 2024 from IP address 117.98.129.62.

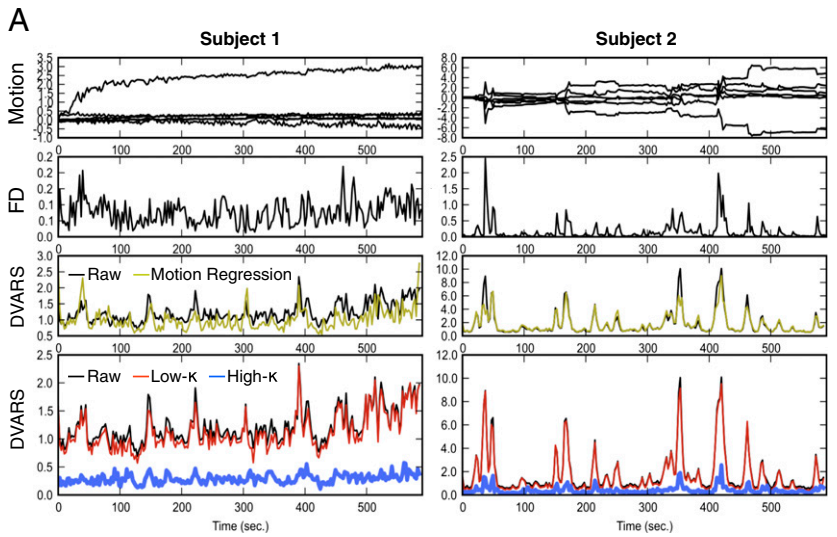

B

i. Acquisition Parameters

	Voxel Size	*TR*
Single-Echo	3x3x3.75	2.26
Multi-Echo (ME)	3.75x3.75x4.4	2.47

ii. Signal Quality

	Preprocessed tSNR	*ICA % Var. Exp.*	*κ*
Single-Echo	130±14%	76±3%	-
Comb. ME	285±10%	85±5%	-
ME-ICA	517±9%	97±1%	80±4%

iii. ME-ICA : Low vs. High Motion

	Comb. ME tSNR[1]	*ME-ICA tSNR*	*BOLD DOF*[2]
Low-Motion	297±7%	548±4%	40±6%
High-Motion	235±4%	529±5%	33±8%

Significant difference between high and low movers: [1]p<0.03 [2]p<0.02

Fig. 1. (*A*) Comparison of two datasets (subjects 1 and 2) with increasing levels of in-scanner head motion. For each subject, four panels show (from top to bottom) rigid-body MP traces in millimeter units; FD traces; a comparison of DVARS for raw data (black trace) and motion regressed data; and comparison of DVARS for raw data (black trace) and high and low-κ time series (blue and red traces, respectively) from ME-ICA. The MP traces show that subjects have (left to right) repeated small movements atop a more substantial tilt (>3 mm maximum) and a series of large abrupt head movements of >3 mm in some directions and >1–2 mm in FD. Subject 2 is a worst-case dataset that would ordinarily be discarded, but is studied here as a test case. For all subjects, DVARS traces show that linear regression of motion parameters (and first derivatives) does not effectively remove most motion-related signals. In contrast, low-κ time series capture the majority of motion-related signals, leaving a comparatively flat DVARS trace from high-κ time series without the use of motion parameter regression or band pass filtering. (*B*) Comparison of acquisition parameters (*i*) and signal quality after preprocessing for conventional methods vs. ME acquisition and ME-ICA denoising (*ii*). ME acquisition has larger voxels and longer repetition time (TR), but T_2^* weighted combination gives greater than expected increases in tSNR (190 theoretical based on voxel size increases). ME-ICA denoising nearly quadruples tSNR while explaining nearly all (97%) combined ME variance. Number of high-κ components differs significantly between high- and low-motion subject groups (*iii*).

used to identify non-BOLD signal changes, measured using the pseudo-*F*-statistic ρ (see *SI Theory* for theory summary). In this framework, denoising involves removing low-κ/high-ρ components from data, which theoretically includes all non-BOLD signals including motion artifacts (see Fig. S1 for selection example). This approach enables comprehensive denoising with minimal operator intervention and without additional arbitrary preprocessing steps. We then describe an estimator of functional connectivity based on interregional correlation between the coefficients of BOLD independent components. Because these components are, by construction, independent, this means that the BOLD degrees of freedom for inference are known and can be used to appropriately normalize correlation values (12, 13). This normalization also controls for variability in BOLD degrees of freedom due to varying BOLD sensitivity with subject motion (14). We show that this approach, called ME independent components regression (ME-ICR), supports valid hypothesis testing of functional connectivity for individual subject data and groups of data. By analyzing data from healthy volunteers exhibiting a wide variety of noncompliant motion, we show that ME-ICA denoising leads to substantial improvements in signal-to-noise ratio over conventional single-echo techniques. We then show that ME-ICR yields valid statistical inference with nominal type 1 error control and the generation of plausible and specific maps of functionally connected brain regions at multiple levels of analysis.

Results

ME-ICA Motion Artifact Removal. We first assessed the capability of ME-ICA denoising to attenuate movement-related effects on time series. ME-ICA denoising involved separating a raw (optimally combined; *SI Materials and Methods*; Fig. S2) ME-fMRI time series dataset into separate BOLD (high-κ) and non-BOLD (low-κ) time series datasets (11) (*SI Materials and Methods*). Theoretically, and on the basis of prior results, we expected that the high-κ time series would represent functional activity generating BOLD contrast (see Fig. S3 for functional component maps), whereas the low-κ time series would represent other sources of non-BOLD variance such as head movement artifact (see Fig. S4 for denoised time series). ME-ICA denoising and conventional denoising are compared for the same ME datasets. Conventional denoising involved regression of motion parameters (MPs), high-pass filtering, and despiking (see *SI Materials and Methods* for ordering). Denoising performance is demonstrated for two individual datasets exhibiting different patterns of noncompliant head movement (Fig. 1*A*). Head motion parameters for subject 1 (low motion) show a prolonged, gradual drift in head position over the course of scanning; subject 2 (high motion) moved to a greater extent (up to 8 mm total displacement) and more abruptly at times.

Additional diagnostics from other studies were used here to characterize in more detail the extent of transient head movements, their impact on fMRI signal variance, and denoising performance in terms of uncoupling BOLD signals from transient, nonlinear head motion artifacts. Framewise displacement (FD), computed as the sum of motion parameter first derivatives, measured the occurrence of transient movements. Delta variation signal (DVARS), computed as the root mean square (RMS) average of the first derivatives of all fMRI signals, identified time points with rapidly changing fMRI signal (2). Correspondence or coupling of DVARS and FD traces indicated contamination of fMRI signals with motion artifacts (*SI Materials and Methods*). For example, the high motion dataset is affected by numerous transient increases in FD (e.g., at 50 and 420 s) that are associated with increases in DVARS, indicating that subject motion produced bursts of rapidly changing fMRI signal. By the same token, uncoupling of FD and DVARS traces indicated effective denoising for movement effects. DVARS processes for conventionally denoised data closely overlapped with DVARS processes for raw data, indicating that linear motion parameter regression was ineffective. Because most motion artifact remains in data after linear regression, this suggests that most motion artifacts are nonlinear manifestations of head motion parameters. In comparison, DVARS traces for high κ time series are essentially flat, indicating the removal of both linear and nonlinear effects of motion. On the other hand, DVARS traces for low κ time series closely match DVARS traces for raw data. This

Downloaded from https://www.pnas.org by 117.98.129.62 on December 26, 2024 from IP address 117.98.129.62.

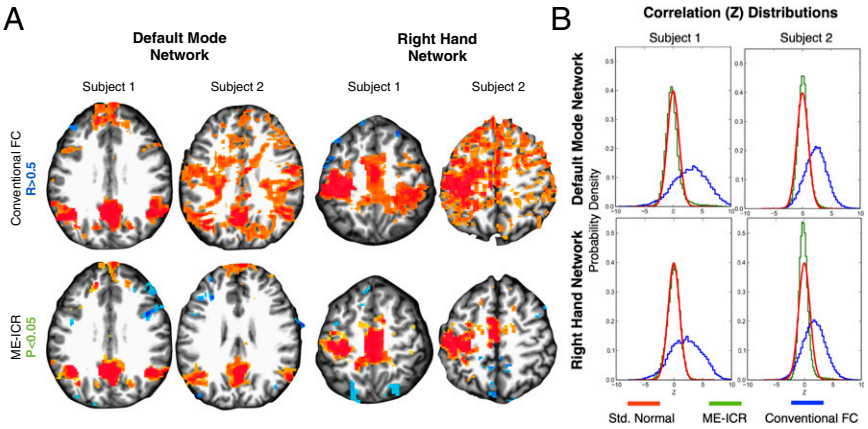

Fig. 2. (*A*) Maps for seed-based correlation analysis after conventional denoising and functional connectivity estimation (top row) and ME-ICR (bottom row). Conventional connectivity maps are thresholded to $R > 0.5$ and ME-ICR maps are thresholded to $P < 0.05$. Connectivity is shown for the default mode network (*Left*) and right hand area (*Right*) in two subjects with moderate and high levels of motion, respectively (1 and 2 from Fig. 1). (*B*) Probability densities of functional connectivity values (Z) for seed-based connectivity analysis after conventional (blue), ME-ICA analysis (green), and a standard normal distribution (red) for comparison. Left side of axial images correspond to anatomical left.

distinction indicates that ME-ICA specifically isolates motion artifacts as non-BOLD signals. These results illustrate that removing non-BOLD signals is a more effective means of removing motion artifact than linear regression of head movement parameters while also reiterating that other non-BOLD artifacts such as cardiac pulsation can be removed equivalently (11).

To evaluate the denoising performance of ME-ICA more rigorously, gray matter temporal signal to noise (tSNR) was measured to assess BOLD sensitivity (Fig. 1*B*, *i* and *ii*; see *SI Materials and Methods* for computation details). High-κ time series were compared with corresponding conventionally denoised optimally combined ME time series (as above). In addition, the tSNR of standard single-echo fMRI (without parallel imaging) was also assessed using conventional denoising. This experiment was conducted for three representative subjects. ME-ICA high-κ time series had a mean tSNR of 517 with 9% uncertainty. Because ME-ICA decomposition explained 97% of dataset variance on average, this significantly increased tSNR fairly represented acquired signals (*SI Theory*). Conventionally denoised ME data had approximately half that tSNR, at 285, with similar uncertainty. Finally, conventionally denoised single-echo data had a tSNR of 130 with 14% uncertainty. Importantly, these results show that the pulse sequence techniques used to acquire ME fMRI, such as parallel imaging, ultimately lead to improved signal quality for ME data over single-echo data. In conjunction with ME-ICA, acquiring ME data leads to a fourfold improvement in data quality over conventional fMRI acquisition and standard denoising techniques.

The hypothesis that subject motion reduced BOLD sensitivity and effective BOLD degrees of freedom was assessed next. BOLD sensitivity was assessed in terms of tSNR, and degrees of freedom were estimated as the number of high-κ components. In this experiment, the main cohort of 32 subjects was divided into high and low motion groups by median split according to a measure of total motion, computed as the sum of FD. The tSNR of conventionally preprocessed ME data was compared between groups to estimate the effect of motion without ME-ICA (Fig. 1*B, iii*). Results showed that even in high tSNR data such as combined ME data, high motion datasets had ∼25% lower tSNR than low motion datasets, which was a significant difference ($P < 0.03$). Based on the DVARS experiment, this limitation to BOLD sensitivity can be attributed to residual motion artifact signals in data. In the high-κ time series resulting from ME-ICA denoising, there was no significant difference in tSNR, due to comparable artifact removal from datasets with different levels of motion. However, high motion ME data still had significantly fewer degrees of freedom according to ME-ICA ($P < 0.02$), likely due to the physical processes underlying artifacts interfering with the BOLD contrast mechanism and thus reducing functionally related BOLD signal variability (Fig. S5).

Subject Level ME-ICR Seed Connectivity Estimation. After ME-ICA selected functionally related BOLD-independent components and counted BOLD degrees of freedom, ME-ICR was used to estimate functional connectivity. For each dataset, ME-ICR estimated functional connectivity as the Pearson correlation of high-κ, BOLD-weighted independent component (IC) coefficients. These IC coefficient correlations were converted to standard scores (Z) using the Fisher transform for the appropriate degrees of freedom, i.e., simply the number of BOLD independent component coefficients (*SI Materials and Methods*). ME-ICR connectivity was compared with conventional seed-connectivity mapping using Pearson correlation of time series that were conventionally denoised (motion parameter regression, despiking, 0.02- to 0.1-Hz band-pass filtering). Conventional correlation values were converted to standard scores using the Fisher transform for 82 nominal degrees of freedom. Because valid inference is not ordinarily expected of conventional functional connectivity analysis of individual resting fMRI datasets, conventional connectivity maps were thresholded to $R > 0.5$. In contrast, valid inference was expected for ME-ICR connectivity, so these maps were thresholded to nominal $P < 0.05$ based on Z-score. Corrections for multiple comparisons using stronger thresholds [false discovery rate (FDR); $q < 0.01$] yielded similar maps, indicating the robustness of the present connectivity estimation method (Fig. 2*A*).

ME-ICR connectivity estimation was expected to produce more consistent connectivity maps than conventional connectivity estimation across datasets with varying subject motion. This hypothesis was tested using the low and high motion datasets referenced in Fig. 1*A*. Subject 1 (low motion) expressed 32 BOLD degrees of freedom, whereas subject 2 (high motion) expressed 13, emphasizing the deleterious effect of motion on BOLD sensitivity. For both subjects, a posterior cingulate cortex seed was used to map the default mode network, and a right hand area seed was used to map the right hand motor network. For each seed, results compare connectivity maps across subject and method. Using conventional connectivity estimation, maps across low and high motion subjects are not clearly comparable. Increased correlation across gray and white matter and apparent underthresholding for subject 2 are associated with residual motion artifact and decreased effective degrees of freedom. In comparing conventional and ME-ICR connectivity for subject 1, maps were similar except for the right hand network having attenuated contralateral sensory cortex connectivity. For subject 2, ME-ICR estimation generated maps with much lower noise than conventional connectivity maps. Finally, comparing ME-ICR connectivity for subjects 1 and 2 shows consistent ME-ICR maps despite significant differences in subject motion and BOLD degrees of freedom.

The capability for inference using ME-ICR was further examined using probability density histograms for correlation values (Fig. 2*B*). One histogram is given per subject and per seed.

Downloaded from https://www.pnas.org by 117.98.129.62 on December 26, 2024 from IP address 117.98.129.62.

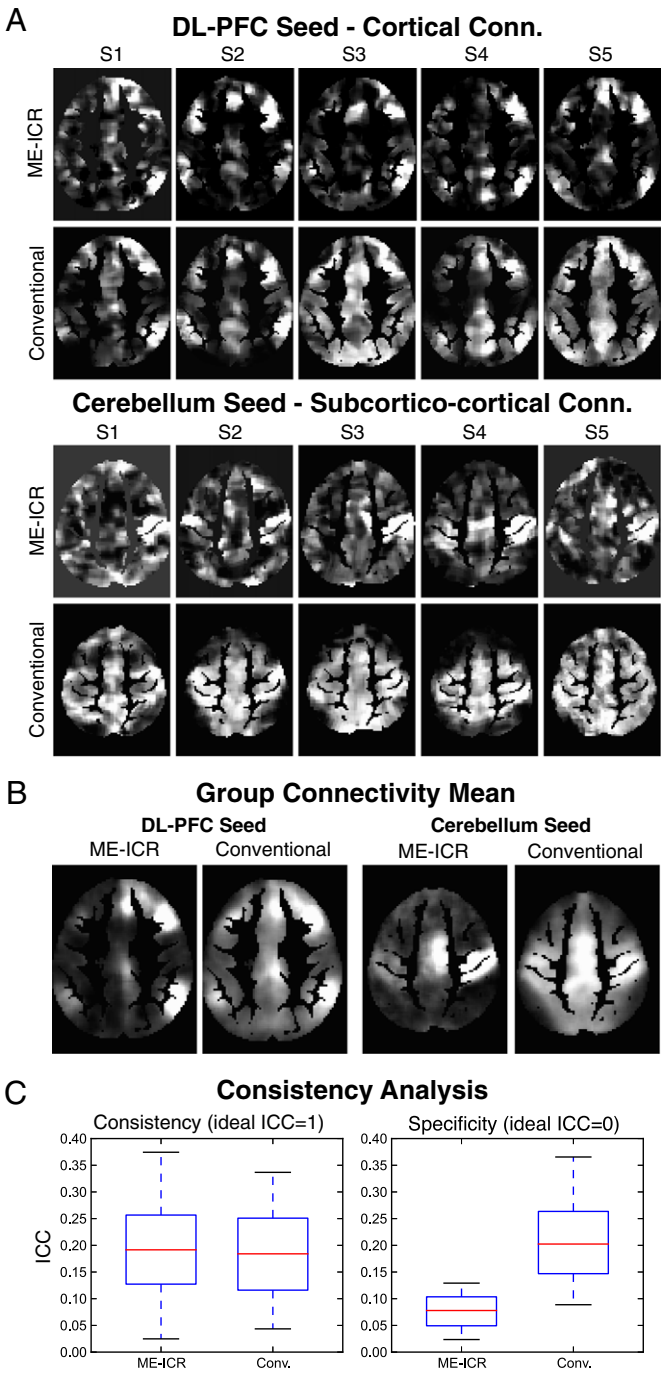

Fig. 3. (*A*) Unthresholded maps of ME-ICR and conventional connectivity maps using seeds: right DL-PFC and left cerebellar motor area seeds, to assess cortical and subcortical-cortical connectivity respectively. (*B*) Mean connectivity maps for both estimators and both seeds. (*C*) Consistency analysis of ME-ICR and conventional connectivity. Consistency is assessed using ICC of connectivity for individual seeds over 32 subjects. ICC = 1 is ideal, indicating seed connectivity is identical over subjects. Specificity is assessed using ICC of connectivity for individual subjects over 32 random seeds. ICC = 0 is ideal, indicating random connectivity maps are not consistent. Left side of axial images correspond to anatomical left.

Each histogram compares a standard normal distribution with ME-ICR and conventional connectivity distributions. It is apparent that across subject and seed, ME-ICR follows the standard normal distribution, varying with heavy right tails and differences in kurtosis. In contrast, conventional connectivity distributions are more variable and result in right-shifted distributions (6). The centered distribution of ME-ICR connectivity is expected because spatial ICA components are uncorrelated, and the standard variance of the distribution indicates that the number of independent component coefficients is indeed an appropriate estimator of the degrees of freedom in BOLD signals. Altogether, ME-ICR distributions indicate that conventional statistical inference for individual subject connectivity is valid in this mode of functional connectivity estimation.

Consistency and Specificity of ME-ICR Connectivity. The consistency of seed connectivity maps from ME-ICR vs. conventional connectivity was compared. Connectivity maps were computed for individual subjects using right dorsolateral prefrontal cortex (DL-PFC) and left cerebellar motor area seeds; unthresholded maps from both estimators are shown for five random subjects (Fig. 3*A*). These particular seeds were chosen because they have lateralized connectivity (useful for inferring specificity). Cerebellar motor area connectivity is particularly informative because it is between contralateral cortical and subcortical areas, which have significantly different tSNR. In ME-ICR maps across subjects, consistent DL-PFC connectivity is seen between middle frontal gyrus and ipsilateral inferior parietal cortex, showing near-0 connectivity for other regions. Right cerebellar motor area connectivity is seen to the contralateral cortical motor area with similar specificity. In contrast, conventional connectivity maps vary from showing the aforementioned regionally specific connectivity to showing diffuse connectivity across the brain. Mean connectivity maps (across all subjects) indicated overall that conventional connectivity had low functional contrast (Fig. 3*B*). This attribute is highlighted by connectivity between the right cerebellar motor area and contralateral cortical motor area. Where contralateral subcortical–cortical connectivity cannot be seen in conventional connectivity maps, it is clearly shown by ME-ICR.

ME-ICR and conventional connectivity were assessed for consistency and specificity (Fig. 3*C*) in subject-level connectivity for random seeds using the intraclass correlation coefficient (ICC; *SI Materials and Methods*) (15). Consistency was assessed by computing the ICC of connectivity maps for the same seed over subjects. In this comparison, ideal ICC = 1; however, lower is expected due to random error and intersubject variability. Specificity was assessed by computing ICC of maps for the same subject over random seeds. In this comparison, ideal ICC = 0, because random maps should have little consistency. Thirty-two random gray matter seeds were analyzed to match the number of subjects in the analysis. Conventional connectivity showed no significant difference in ICC across maps from random subjects vs. maps from random seeds, indicating poor specificity. ME-ICR connectivity, in contrast, showed significant difference between the two factors. ME-ICR and conventional connectivity maps across subjects did show nominally similar consistency according to ICC values, but because conventional connectivity had the same mean ICC over random maps, its apparent consistency is not significant. The ratio of mean ICC values shows that ME-ICR at least doubles specificity over conventional seed-connectivity analysis.

Group Level Connectivity. After confirming the statistical conditioning of subject-level connectivity values from ME-ICR and their consistency across subjects, ME-ICR group analysis was conducted using one-sample t tests of ME-ICR connectivity maps across subjects for four commonly studied seed regions: posterior cingulate cortex, right hand area, Broca's area, and left V1 (Fig. 4*A*). Similarly, conventional group analysis was conducted using one-sample t tests of conventional connectivity maps across subjects for the same seeds (*SI Materials and Methods*). Group connectivity maps were thresholded according to t-value. When thresholding conventional connectivity maps, all common significance values ($P < 0.05$–10^{-5}) led to essentially fully populated maps. Conventional group connectivity maps had to be thresholded at $P < 10^{-7}$ before interpretable maps were produced; this P value corresponded to an FDR-corrected

Downloaded from https://www.pnas.org by 117.98.129.62 on December 26, 2024 from IP address 117.98.129.62.

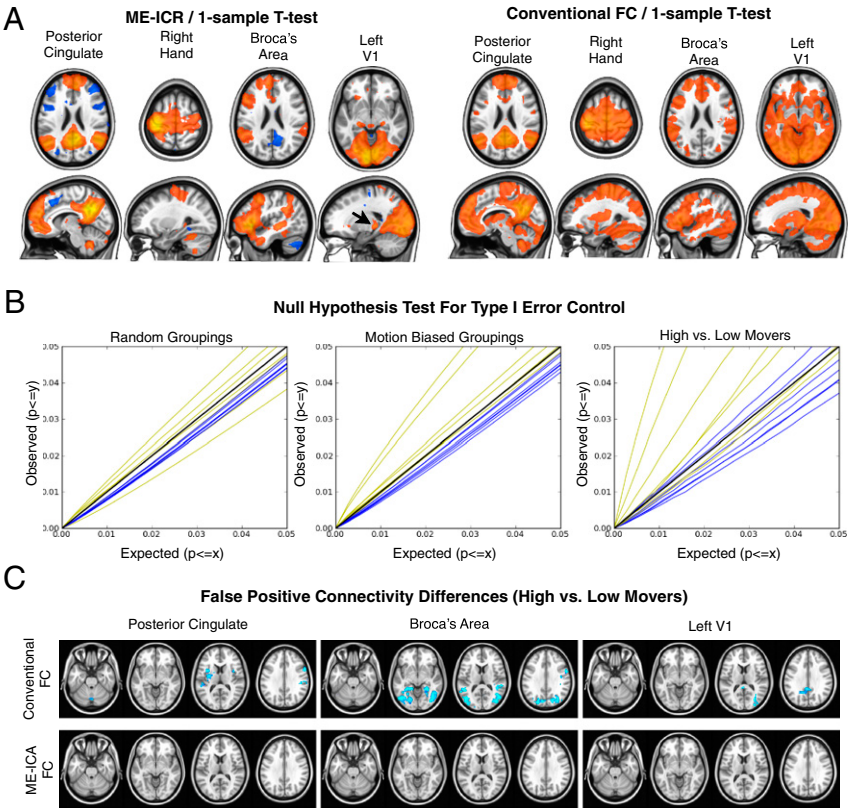

Fig. 4. (*A*) Group-level connectivity maps using ME-ICR ($P < 0.001$, FDR q < 0.005) and conventional connectivity ($P < 10^{-7}$, FDR q < 10^{-6}) for four different seeds: posterior cingulate, right hand, Brocas area, and left V1. ME-ICR connectivity shows for the PCC, the canonical default mode network; for the right hand, ipsilateral motor and premotor areas, bilateral sensory cortices, ipsilateral thalamus, and contralateral cerebellum; for Broca's area, premotor, middle temporal, supramarginal areas, and ipsilateral dorsal striatum; and for visual seed, bilateral visual cortices bounded by parieto-occipital junction and the pulvinar of the thalamus (black arrow). Conventional connectivity shows for PCC, connectivity to the motor cortex; for the right hand to the insula; for Brocas area, bilateral connectivity; and for primary visual cortex, the whole cortex. (*B*) For regions in *A*, plus dorsolateral, ventromedial prefrontal cortices, caudate, and insula, type I error control for contrasts between subgroupings: random (*Left*); motion biased (*Center*); high vs. low movers (*Right*). For each seed, observed error (*y* axis) compared with expected error (*x* axis). Comparisons are made at a series of significance values (lines, 0.0001–0.05), for ME-ICR (blue) and conventional (yellow) connectivity. Lines below and above $y = x$ (black line) denote nominal and failed type I error control, respectively. ME-ICA consistently demonstrates nominal type I error control, whereas in biased and extreme cases, conventional connectivity fails with up to five times greater type I error than expected. (*C*) Maps of false-positive connectivity differences between high vs. low movers after thresholding to $P < 0.01$ and familywise error (cluster) correction to <0.05. All conventional FC maps are populated by false-positive clusters. All ME-ICR maps are empty. Left side of axial images correspond to anatomical left.

significance of $q < 10^{-6}$, suggesting overestimated statistical significance. Moreover, thresholded conventional group connectivity maps often appeared globally significant, reflecting the nonspecificity of the conventional connectivity estimates shown in Fig. 3C. In contrast, group-level ME-ICR connectivity maps at thresholds corresponding to $P < 0.001$ (FDR $q < 0.005$) were comparable to maps observed in subject-level analysis, were consistent with connectivity known from neuroanatomy and task-based fMRI, and indicated comparable levels of plausible connectivity for different seeds. For example, Broca's area connectivity shows the lateralized language network involving left inferior frontal gyrus, Wernicke's area (superior temporal gyrus), and supramarginal gyrus. Conventional connectivity maps show bilateral connectivity without indicating the supramarginal gyrus. Left V1 connectivity specifically follows the temporal-parieto-occipital junction and clearly shows bilateral pulvinar, whereas conventional connectivity is highly unspecific, indicating connectivity to almost all gray matter.

Type I Error Testing of Group Level ME-ICA Functional Connectivity. ME-ICR and conventional connectivity were assessed for false-positive (type I) error control in group contrasts (*SI Materials and Methods*) (16). A null hypothesis test was used, based on computation of functional connectivity contrasts (two-sample *t* tests) between equally sized permuted subgroups of the healthy volunteers for six seed regions. Three subgroupings were assessed: random (50 permutations), partially motion biased (at least half of subjects with greater motion, 50 permutations), and fully motion biased (high vs. low movers). Because subgroups were drawn from the same normal sample, all positive tests were type I error, and the number of false-positive tests was not expected to exceed the number of false-positive tests (*FP*) predicted under the null hypothesis, i.e., $FP = p \times N$, where N is the number of tests and p is the probability of type 1 error (16). False-positive counts were made at 20 thresholds spanning $P = 0.0001$–0.05 (Fig. 4*B*). False-positive counts were pooled over permutations and expressed as an observed false-positive rate and then compared with the expected false-positive rates (p).

For contrasts without motion bias, ME-ICR produced clear and consistent nominal type I error control for all seeds. Conventional functional connectivity had more varied performance, in that observed rates could exceed expected rates by small but notable margins. In subgroupings biased by motion, ME-ICR continued to exercise nominal type 1 error control. In contrast, conventional connectivity contrasts clearly failed in error control, with observed error rates up to twice the expected rate. Last, in the extreme case of contrast between functional connectivity maps for high movers vs. low movers (Fig. 4*C*), ME-ICR again maintained nominal type I error control, whereas observed false-positive rates for conventional connectivity testing were up to five times the expected rate. Results therefore show the crucial finding that group-level ME-ICR connectivity contrasts have nominal type I error control that is highly robust to biases in subject motion.

Discussion

Eliminating spurious seed-connectivity findings requires both robust BOLD denoising and valid statistical estimation and inference. Conventional functional connectivity methodology works within the limitations of single-echo fMRI to achieve specific goals in denoising or connectivity estimation. Isolating BOLD signals with ME-ICA allows several established goals to be achieved simultaneously. The tSNR of signal was greatly increased over conventional methods using widely available MRI hardware. Motion artifacts were removed without motion parameter regression or scrubbing. Band-pass filtering was removed from analysis, and spatial ICA transformation represented the full-frequency spectrum of BOLD signals for seed-connectivity analysis with ME-ICR. The positive bias of conventional subject-level connectivity did not affect ME-ICR, so the problems of distribution centering with global signal regression were avoided (6). Subject-level connectivity inference with ME-ICR was consistent across datasets with significant differences in motion.

Downloaded from https://www.pnas.org by 117.98.129.62 on December 26, 2024 from IP address 117.98.129.62.

The poor specificity of conventional seed-connectivity was characterized, and ME-ICR doubled specificity, at least. Conventional group-level seed-connectivity maps were characterized as having diffuse and neuro-anatomically inaccurate global connectivity. This limitation of conventional analysis was due to its poor specificity in mapping anatomically predictable patterns of cortical–cortical and cortical–subcortical connectivity. Conventional connectivity differences between groups with different motion were associated with up to fivefold greater type I error than expected under the null hypothesis. In contrast, ME-ICR produced precise and plausible connectivity maps based on valid statistical inference across subject and group levels of analysis, critically culminating in type I error rates predicted by the null hypothesis for explicitly motion-biased group contrasts. Altogether, preprocessing was greatly simplified and made more effective, and valid hypothesis testing was enabled for the study of connectivity differences between groups with motion differences.

The present study leveraged many benefits of ICA for resting state fMRI analysis. To date, ICA has been applied in both spatial and temporal domains to produce connectivity maps (17). Spatial ICA has shown common components across subjects and has been used to find the common set of components across groups. Dual regression of spatial ICA maps also enables the study of group differences in shared components (18). Here we use spatial ICA as a transformation of BOLD signals for ME-ICR. This method essentially is principal component regression in the space of the BOLD-weighted independent components. Functional connectivity estimation and inference with ME-ICR is an important contribution to ICA methodology because it enables subject- and group-level hypothesis testing without expert knowledge for component selection or a shared basis of connectivity maps. These attributes make ME-ICR well suited to studying patient populations with poorly characterized functional networks and in computing connectivity differences between healthy volunteers and patients that may not share the same basis of functional networks.

The limitations of ME-ICR relate to ME acquisition, ICA, and TE-dependence analysis. Current ME fMRI implementations use parallel imaging to acquire images at multiple TEs. Parallel imaging may increase susceptibility to motion artifacts, but we have shown that, regardless, the proposed approach improves tSNR and reduces artifacts over conventional methods. ME acquisition achieves better signal quality at the cost of lower temporal and spatial resolution than conventional acquisition. Single-echo multiband imaging may allow also denoising and tSNR increases with better resolution (19, 20). However, approaches that do not isolate BOLD signals would still require the application of various filters for denoising and would not solve problems of seed-connectivity inference.

Materials and Methods

fMRI Data Acquisition. This study was approved by the Local Research Ethical Committee at the University of Cambridge (LREC 11/EE/0198). Resting state fMRI data were acquired from 35 normal consenting volunteers (18 men and 17 women; mean age, 33 ± 13 y). Data were acquired with a Siemens Trio 3T MRI Scanner and a 32-channel receive-only head coil (Siemens Medical Solutions). Functional images were acquired with an ME EPI sequence with online reconstruction [repetition time (TR), 2.47 s; flip angle, 78°; matrix size, 64 × 64; in-plane resolution, 3.75 mm; field of view (FOV), 240 mm; 32 oblique slices, alternating slice acquisition slice thickness 3.75 mm with 10% gap; iPAT factor, 3; bandwidth (BW) = 1,698 Hz/pixel; TE = 12, 28, 44, and 60 ms] (9). For three subjects, an additional single-echo EPI scan was acquired (TR, 2.26 s; flip angle, 78°; matrix size, 64 × 64; in-plane resolution, 3.0 mm; FOV, 192 mm; 32 oblique slices, alternating slice acquisition slice thickness, 3.75; iPAT factor, 3; TE = 30 ms). Anatomical images were acquired using a T1-weighted magnetization prepared rapid gradient echo (MPRAGE) sequence [176 × 240 FOV; 1-mm in-plane resolution; inversion time (TI), 1,100 ms]. Preprocessing and ME-ICA for denoising and BOLD component identification was performed with the AFNI tool meica.py (11, 21). Anatomical and functional data were nonlinearly warped to the MNI template using FSL FNIRT (22). See *SI Materials and Methods* for further processing details.

ME-ICR. Subject-level seed-based connectivity analysis for ME-ICA processed BOLD component coefficients was based on computing the Pearson correlation of spatial ICA component coefficients. The ICA mixing matrix was fit to the T_2^* weighted combination of ME data (9), and the coefficient maps corresponding to high-κ components comprised the component coefficient dataset. Following computation of correlation between vectors of component coefficients, Pearson's R values were converted to standard (Z) scores using the Fisher R-Z transform, with degrees of freedom counted as the number of high-κ components.

ACKNOWLEDGMENTS. P.K. is supported by the National Institutes of Health–Cambridge Scholars Program. V.V. is a Wellcome Trust Clinical Fellow. fMRI data collection was supported by the National Institute of Health Research Cambridge Biomedical Research Centre.

1. Biswal B, Yetkin FZ, Haughton VM, Hyde JS (1995) Functional connectivity in the motor cortex of resting human brain using echo-planar MRI. *Magn Reson Med* 34(4):537–541.
2. Power JD, Barnes KA, Snyder AZ, Schlaggar BL, Petersen SE (2012) Spurious but systematic correlations in functional connectivity MRI networks arise from subject motion. *Neuroimage* 59(3):2142–2154.
3. Satterthwaite TD, et al. (2012) Impact of in-scanner head motion on multiple measures of functional connectivity: Relevance for studies of neurodevelopment in youth. *Neuroimage* 60(1):623–632.
4. Van Dijk KRA, Sabuncu MR, Buckner RL (2012) The influence of head motion on intrinsic functional connectivity MRI. *Neuroimage* 59(1):431–438.
5. Satterthwaite TD, et al. (2013) An improved framework for confound regression and filtering for control of motion artifact in the preprocessing of resting-state functional connectivity data. *Neuroimage* 64(1):240–256.
6. Murphy K, Birn RM, Handwerker DA, Jones TB, Bandettini PA (2009) The impact of global signal regression on resting state correlations: Are anti-correlated networks introduced? *Neuroimage* 44(3):893–905.
7. Saad ZS, et al. (2012) Trouble at rest: How correlation patterns and group differences become distorted after global signal regression *Brain Connectivity* 2(1):25–32.
8. Salvador R, et al. (2008) A simple view of the brain through a frequency-specific functional connectivity measure. *Neuroimage* 39(1):279–289.
9. Poser BA, Versluis MJ, Hoogduin JM, Norris DG (2006) BOLD contrast sensitivity enhancement and artifact reduction with multiecho EPI: Parallel-acquired inhomogeneity-desensitized fMRI. *Magn Reson Med* 55(6):1227–1235.
10. Peltier SJ, Noll DC (2002) T(2)(*) dependence of low frequency functional connectivity. *Neuroimage* 16(4):985–992.
11. Kundu P, Inati SJ, Evans JW, Luh WM, Bandettini PA (2012) Differentiating BOLD and non-BOLD signals in fMRI time series using multi-echo EPI. *Neuroimage* 60(3):1759–1770.
12. Hyvärinen A, Oja E (2000) Independent component analysis: Algorithms and applications. *Neural Netw* 13(4–5):411–430.
13. Beckmann CF, Smith SM (2004) Probabilistic independent component analysis for functional magnetic resonance imaging. *IEEE Trans Med Imaging* 23(2):137–152.
14. Friston KJ, et al. (1995) Analysis of fMRI time-series revisited. *Neuroimage* 2(1):45–53.
15. Bartko JJ (1966) The intraclass correlation coefficient as a measure of reliability. *Psychol Rep* 19(1):3–11.
16. Bullmore ET, et al. (1999) Global, voxel, and cluster tests, by theory and permutation, for a difference between two groups of structural MR images of the brain. *IEEE Trans Med Imaging* 18(1):32–42.
17. Smith SM, et al. (2012) Temporally-independent functional modes of spontaneous brain activity. *Proc Natl Acad Sci USA* 109(8):3131–3136.
18. Filippini N, et al. (2009) Distinct patterns of brain activity in young carriers of the APOE-ε4 allele. *Proc Natl Acad Sci USA* 106(17):7209–7214.
19. Setsompop K, et al. (2012) Blipped-controlled aliasing in parallel imaging for simultaneous multislice echo planar imaging with reduced g-factor penalty. *Magn Reson Med* 67(5):1210–1224.
20. Feinberg DA, et al. (2010) Multiplexed echo planar imaging for sub-second whole brain FMRI and fast diffusion imaging. *PLoS ONE* 5(12):e15710.
21. Cox RW (1996) AFNI: Software for analysis and visualization of functional magnetic resonance neuroimages. *Comput Biomed Res* 29(3):162–173.
22. Klein A, et al. (2009) Evaluation of 14 nonlinear deformation algorithms applied to human brain MRI registration. *Neuroimage* 46(3):786–802.

Downloaded from https://www.pnas.org by 117.98.129.62 on December 26, 2024 from IP address 117.98.129.62.